Supplementing Information
for
Tracking recent extremes and interannual variability of global fire emissions using a near-real-time extension to the Global Fire Emissions Database

[1]Yang Chen, [2]Guido R. van der Werf, [1]Mingquan Mu, [3]Dave van Wees, [4]Joanne V. Hall, [4]Louis Giglio, [2]Roland Vernooij, [5]Douglas C. Morton, [1]Li Xu, [6]Tianjia Liu, [1]Rebecca C. Scholten, [7]Shane R. Coffield, [5]Melanie B. Follette-Cook, [5]Lesley Ott, [1]James T. Randerson

[1]Department of Earth System Science, University of California, Irvine, 92612, USA
[2]Meteorology and Air Quality Group, Wageningen University & Research, Wageningen, the Netherlands
[3]BeZero Carbon, London, UK
[4]Department of Geographical Sciences, University of Maryland, College Park, MD, USA
[5]Biospheric Sciences Laboratory, NASA Goddard Space Flight Center, Greenbelt, MD, USA
[6]Department of Geography, University of British Columbia, Vancouver, BC, Canada
[7]Earth System Science Interdisciplinary Center, University of Maryland, College Park, MD, USA

Table of Contents

SI Tables: Table S1-S6

SI Figures: Figure S1-S8

SI Texts: Text S1-S4

References

SI Tables (S1-S6)

Table S1. Summary of annual global (a) burned area (Mha yr^{-1}) and (b) fire emissions (Pg C yr^{-1}) from different GFED versions. Values represent means over each dataset's full study period. For GFED5 (including versions 5.0 and 5.1), additional mean values calculated for the MODIS era (post-2002) are shown in parentheses.

(a) Burned area (Mha yr^{-1})

	GFED **version** and *reference*					
Year	**GFED1** *Giglio et al (2006)*	**GFED2** *van der Werf et al. (2006)*	**GFED3** *Giglio et al. (2010)*	**GFED4s** *van der Werf et al. (2017)*	**GFED5.0** *Chen et al. (2023)*	**GFED5.1** *van der Werf et al. (2025)*
1997		338	360	489	749	753
1998		372	431	546	921	920
1999		341	409	516	791	782
2000		358	394	491	833	831
2001	374	374	372	543	915	921
2002	351	351	386	534	851	859
2003	297	297	346	473	814	817
2004	319	319	363	499	852	854
2005			357	494	824	827
2006			342	468	768	770
2007			366	496	822	826
2008			330	462	819	822
2009				430	758	761
2010				449	756	758
2011				491	795	798
2012				483	788	791
2013				401	696	699
2014				424	723	725
2015				420	743	745
2016				400	737	740
2017					732	735
2018					684	686
2019					680	683
2020					721	724
2021						687
2022						621
Mean	335	344	371	475	782 (774)	772 (759)

(b) Emissions (Pg C yr^{-1})

	GFED **version** and *reference*			
Year	**GFED2** *van der Werf et al. (2006)*	**GFED3** *van der Werf et al. (2010)*	**GFED4s** *van der Werf et al. (2017)*	**GFED5.1** *van der Werf et al. (2025)*
1997	2.99	2.71	3.03	3.95
1998	3.18	2.78	2.89	4.44
1999	2.28	1.90	2.23	3.40
2000	2.04	1.67	1.90	3.43
2001	2.22	1.56	1.96	3.29
2002	2.39	2.07	2.34	3.28
2003	2.25	2.12	2.20	3.55

2004	2.32	1.97	2.21	3.63
2005		2.11	2.25	3.56
2006		2.06	2.21	3.33
2007		2.04	2.20	3.40
2008		1.68	1.86	3.27
2009		1.52	1.86	3.20
2010			2.15	3.33
2011			1.87	3.21
2012			2.05	3.65
2013			1.77	3.19
2014			2.05	3.26
2015			2.29	3.67
2016			1.87	3.56
2017				3.26
2018				2.93
2019				3.59
2020				3.52
2021				3.38
2022				2.88
Mean	2.46	2.01	2.16	3.43 (3.36)

Table S2. Aggregation schemes used to generate effective fire area (EFA) and fuel consumption (FC). The schemes differ by spatial scale (*Global*: uniform worldwide; *GFED region*: uniform within each GFED region; *Grid cell*: varies at 0.25° resolution), temporal scale (*All months*: constant throughout the year; *Monthly*: varying by month), and biome or fire-type (*Lumped*: uniform across all types; *Specified*: varying by biome or fire type). The number of degrees of freedom associated with each scheme is given in parentheses. The ***Regftp*** scheme (bolded in the table) is used as the reference configuration in this study. A detailed description of all aggregation schemes is provided in Text S1.

Scheme	**Abbreviation**	**Spatial**			**Temporal**		**Biome + type**	
		Grid cell (720×1400)	GFED region (14)	Global (1)	Monthly (12)	All months (1)	Specified (16)	Lumped (1)
Globally uniform scalar	Glb			●		●		●
Global scalars for each type	Glbftp			●		●	●	
Uniform scalar for each region	Reg		●			●		●
Uniform scalar for each type in each region	**Regftp**		●			●	●	
Uniform scalar for each type in each region, monthly	Regftpmo		●		●		●	
Single scalar for each grid cell	Grid	●				●	●	
Monthly scalars for each grid cell	Gridmo	●			●		●	
Combination of *Gridmo* and *Regftpmo*	Combine	●			●		●	

Table S3. Performance metrics for different aggregation schemes (Table S2), evaluated for individual GFED regions and globally. Metrics are computed from monthly time series (2012-2022) of regionally aggregated burned area derived using the GFED5NRT algorithm with different aggregation schemes, using GFED5 as the reference dataset. The ***Regftp*** scheme (bolded in the table) is adopted as the reference configuration in this study.

Scheme	Globe	BONA	TENA	CEAM	NHSA	SHSA	EURO	MIDE	NHAF	SHAF	BOAS	CEAS	SEAS	EQAS	AUST
	Normalized RMSE														
glb	1.63	14.58	7.32	1.88	1.61	3.01	3.40	4.68	0.92	0.81	5.84	2.70	1.27	5.74	1.83
glbftp	1.32	4.25	4.93	1.55	1.75	2.57	2.73	3.10	0.81	0.87	2.77	2.50	1.29	4.20	1.85
reg	1.32	4.10	3.65	1.51	1.17	1.87	2.89	2.73	0.94	0.83	4.17	2.77	1.27	1.80	1.86
regftp	**1.18**	**2.98**	**2.62**	**1.30**	**1.07**	**1.40**	**2.69**	**2.19**	**0.85**	**0.83**	**3.01**	**2.63**	**1.21**	**1.69**	**1.77**
regftpmo	1.13	2.96	2.41	1.30	1.04	1.38	2.69	2.16	0.83	0.76	2.61	2.70	1.18	1.69	1.80
grid	1.33	8.80	2.48	1.20	0.95	1.43	2.84	2.22	0.77	0.75	6.36	2.73	1.10	1.58	2.23
gridmo	1.38	8.60	2.82	1.23	0.95	1.50	2.88	2.35	0.79	0.76	5.92	2.93	1.09	1.60	2.86
combine	1.09	3.14	2.16	1.16	0.93	1.29	2.55	1.98	0.78	0.68	2.93	2.47	1.08	1.52	2.02
	R^2 (coefficient of determination)														
glb	0.82	0.88	0.54	0.73	0.74	0.70	0.56	0.53	0.87	0.87	0.82	0.55	0.79	0.67	0.82
glbftp	0.83	0.88	0.54	0.73	0.74	0.71	0.56	0.55	0.87	0.87	0.82	0.56	0.80	0.67	0.83
reg	0.82	0.88	0.54	0.73	0.74	0.70	0.56	0.53	0.87	0.87	0.82	0.55	0.79	0.67	0.82
regftp	**0.82**	**0.88**	**0.54**	**0.74**	**0.74**	**0.71**	**0.56**	**0.55**	**0.87**	**0.87**	**0.82**	**0.56**	**0.80**	**0.68**	**0.83**
regftpmo	0.83	0.88	0.54	0.73	0.75	0.70	0.56	0.56	0.87	0.87	0.81	0.56	0.80	0.68	0.83
grid	0.82	0.57	0.53	0.73	0.74	0.70	0.54	0.55	0.87	0.87	0.75	0.55	0.79	0.67	0.82
gridmo	0.81	0.45	0.50	0.73	0.75	0.68	0.51	0.54	0.87	0.87	0.71	0.55	0.80	0.67	0.79
combine	0.83	0.88	0.54	0.74	0.75	0.71	0.56	0.55	0.87	0.87	0.82	0.56	0.80	0.68	0.83
	Bias (%)														
glb	4.55	275.44	160.59	28.91	44.63	76.21	37.03	465.61	-23.22	-8.19	61.42	-0.26	-3.60	194.33	-15.66
glbftp	4.02	44.02	80.49	16.00	61.91	63.31	1.58	100.13	-10.49	2.16	-25.42	-18.61	-4.35	146.27	5.89
reg	2.96	39.25	11.61	-7.46	-7.46	10.35	0.98	50.67	7.80	0.46	5.49	7.99	-2.56	-27.24	-8.98
regftp	**3.51**	**16.00**	**4.35**	**-7.35**	**-3.65**	**2.40**	**2.06**	**10.72**	**8.01**	**0.83**	**21.74**	**2.43**	**-3.72**	**-13.91**	**4.73**
regftpmo	2.69	16.63	8.60	-6.32	-1.87	3.45	2.44	12.24	6.65	-0.79	16.32	4.93	-4.38	-12.78	6.55
grid	8.00	87.56	11.65	-5.52	-1.45	6.15	-0.85	15.56	8.55	0.91	84.18	4.73	-4.15	-9.42	15.32
gridmo	7.74	55.36	12.86	-5.37	-0.18	7.07	-7.87	13.70	9.23	0.06	66.70	7.31	-4.28	-8.82	24.25
combine	3.47	18.04	3.05	-7.84	-1.54	0.72	-6.12	3.87	9.41	-1.03	21.58	-4.54	-5.69	-11.44	12.36

Table S4. Dates of missing standard VIIRS active fire data for SNPP and NOAA-20, based on FIRMS missing-data records (https://firms.modaps.eosdis.nasa.gov/api/missing_data). For SNPP, dates between January 1-19, 2012, which are prior to the first publicly available record on January 20, 2012), are also included.

SATELLITE	YEAR	MONTH	DAY
SNPP	2024	11	3-5
		9	26
		7	10-15, 25-28
		6	1-3
		5	30-31
	2022	8	1-10
		7	27-31
	2012	3	25
		1	1-19
NOAA-20	2024	2	4
	2023	9	30
		7	19-22

Table S5. Comparison of fire activity between the 2023–2024 period (GFED5NRT) and the 2002–2022 baseline (GFED5). Reported metrics include global and regional burned area (Mha yr^{-1}) and fire emissions (Tg C yr^{-1}). Long-term trends are shown with and without the inclusion of 2023–2024 data to illustrate the influence of recent fire seasons. Parenthetical values indicate mean-normalized trends (in percentage).

Region	Burned Area					Fire Emissions				
	Mean±Std (Mha yr^{-1})			Trend (Mha yr^{-2})		Mean±Std (Tg C yr^{-1})			Trend (Tg C yr^{-2})	
	2002-2022	2023	2024	2002-2022	2002-2024	2002-2022	2023	2024	2002-2022	2002-2024
BONA	4±1	19	9	-0.05 (-1.22)	0.17 (3.27)	89±47	567	265	-0.59 (-0.66)	6.19 (5.28)
TENA	7±1	6	8	0.02 (0.24)	0.01 (0.14)	29±10	26	35	0.79 (2.68)	0.63 (2.14)
CEAM	12±2	14	14	-0.11 (-0.90)	-0.04 (-0.35)	88±20	109	127	-0.27 (-0.30)	0.44 (0.48)
NHSA	9±2	10	13	-0.06 (-0.70)	0 (0.03)	35±12	39	62	0.26 (0.74)	0.53 (1.44)
SHSA	53±12	44	61	-1.18 (-2.22)	-0.9 (-1.69)	412±124	427	777	-5.69 (-1.38)	-0.21 (-0.05)
EURO	4±1	2	3	-0.1 (-2.56)	-0.1 (-2.62)	14±4	10	16	-0.09 (-0.64)	-0.09 (-0.65)
MIDE	3±1	3	3	0.01 (0.27)	0.01 (0.22)	6±2	6	7	0.06 (0.88)	0.04 (0.57)
NHAF	237±26	214	236	-3.13 (-1.32)	-2.62 (-1.11)	719±68	697	767	-1.19 (-0.17)	-0.61 (-0.08)
SHAF	241±10	253	268	-0.62 (-0.26)	-0.07 (-0.03)	973±53	1029	1119	1.19 (-0.12)	3.05 (0.31)
BOAS	32±11	23	19	-1.19 (-3.77)	-1.13 (-3.70)	295±127	219	309	2.1 (0.71)	1.01 (0.34)
CEAS	40±12	20	22	-1.59 (-3.96)	-1.62 (-4.19)	79±23	43	45	-2.7 (-3.42)	-2.78 (-3.66)
SEAS	59±8	62	56	0.07 (0.12)	0.05 (0.09)	350±69	391	330	1.18 (0.34)	1.09 (0.31)
EQAS	3±2	3	1	-0.16 (-4.71)	-0.15 (-4.55)	96±89	71	22	-3.55 (-3.71)	-3.75 (-4.11)
AUST	52±19	88	50	-1.1 (-2.12)	-0.51 (-0.95)	167±	254	149	-0.5 (-0.30)	0.29 (0.17)
Globe	**759±63**	**761**	**764**	**-9.22 (-1.22)**	**-6.94 (-0.92)**	**3364±221**	**3888**	**4028**	**-9.07 (-0.27)**	**5.5 (0.16)**

Table S6. Summary of regional extreme fire events in 2023–2024 based on GFED5NRT mean annual fire emissions averaged over the two-year period. The raw anomaly represents the absolute deviation of the 2023–2024 mean emissions from the long-term climatological mean (2002–2022). The standardized anomaly expresses this deviation in units of the climatological standard deviation (Z-score), while the relative anomaly represents the percentage difference relative to the climatological mean.

Event region	Emissions (Tg C/yr)	Emission climatology (Tg C/yr)	Absolute anomaly (Tg C/yr)	Standardized anomaly (Z-score)	Relative anomaly (%)
West Canada	278	33	246	68.1	747
East Canada	25	3	22	25.8	756
Central America	27	10	17	31.2	167
Venezuela	23	11	12	35.7	103
Amazon	172	108	64	16.5	59
East Brazil	26	21	5	5.5	23
Bolivia	196	58	138	47.7	239
East Africa	154	121	33	26.7	27
Congo	493	401	92	30.7	23
SE Africa	144	120	24	17.4	20
Asia Steppe	16	8	7	13.2	90
East Siberia	89	31	58	24.5	187
NE China	4	2	2	19.3	141
SE Asia	180	147	33	12.0	23
West Australia	98	52	46	31.4	88
NE Australia	24	15	9	8.2	58
All events	1949	1142	925	-	81
Other	1877	2222	-345	-	-16
Global	3827	3364	463	2.15	14

SI Figures (S1 – S9)

Figure S1. (a) Weighting factors as a function of VIIRS scan angle (sample numbers 0–6399) were derived from all SNPP VIIRS active fire detections during 2019–2021 to adjust the VIIRS fire counts. The weights were calculated separately by land cover type and time of detection (day or night). Dominant land cover at 0.25° resolution was determined using MODIS land cover data (MCD12Q1) and grouped into four categories: **forest** (*Evergreen Needleleaf Forests*, *Evergreen Broadleaf Forests*, *Deciduous Needleleaf Forests*, *Deciduous Broadleaf Forests*, *Mixed Forests*), **grass** (*Grasslands*), **crop** (*Cropland* and *Cropland/Natural Vegetation Mosaics*), and **other** (all remaining types). The color of the lines represents the month. (b) Example for October 2021 showing how applying the weights (for forest-type, daytime detections) modifies the distribution of gridded VIIRS active fire counts as a function of scan angle.

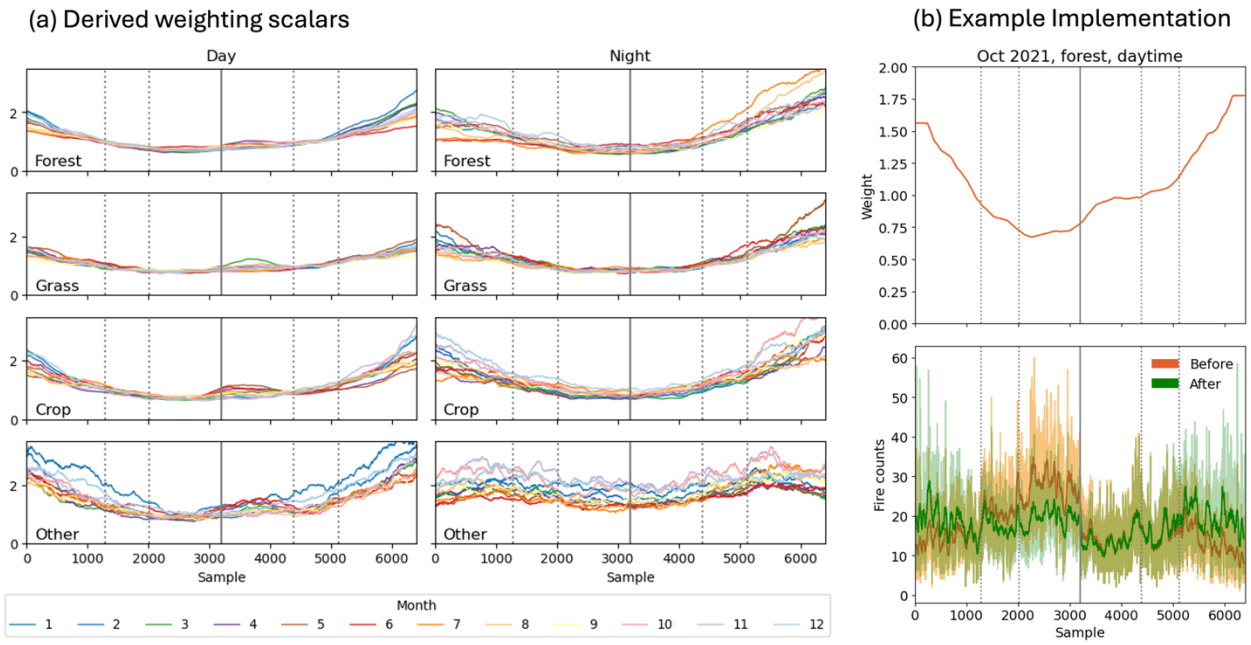

Figure S2. Schematic overview of the operational framework for generating GFED5NRT daily burned area and fire emission products.

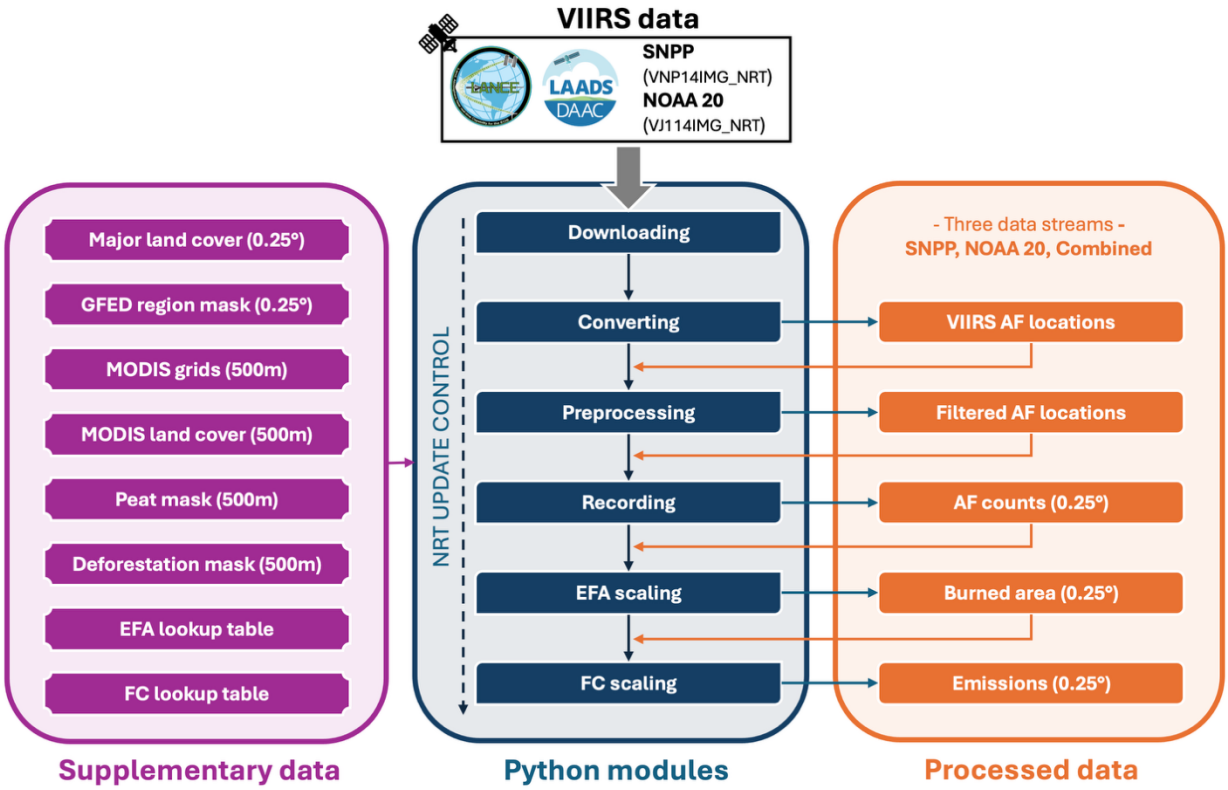

Figure S3. Spatial consistency between 0.25° gridded burned area (BA) from GFED5 and GFED5NRT (using SNPP only), 2012-2022. Each panel represents one year. Black dashed lines indicate the 1:1 relationship, and red lines show the reduced major axis (RMA) regression. The Pearson correlation coefficient (r) and regression slope (m) are also reported.

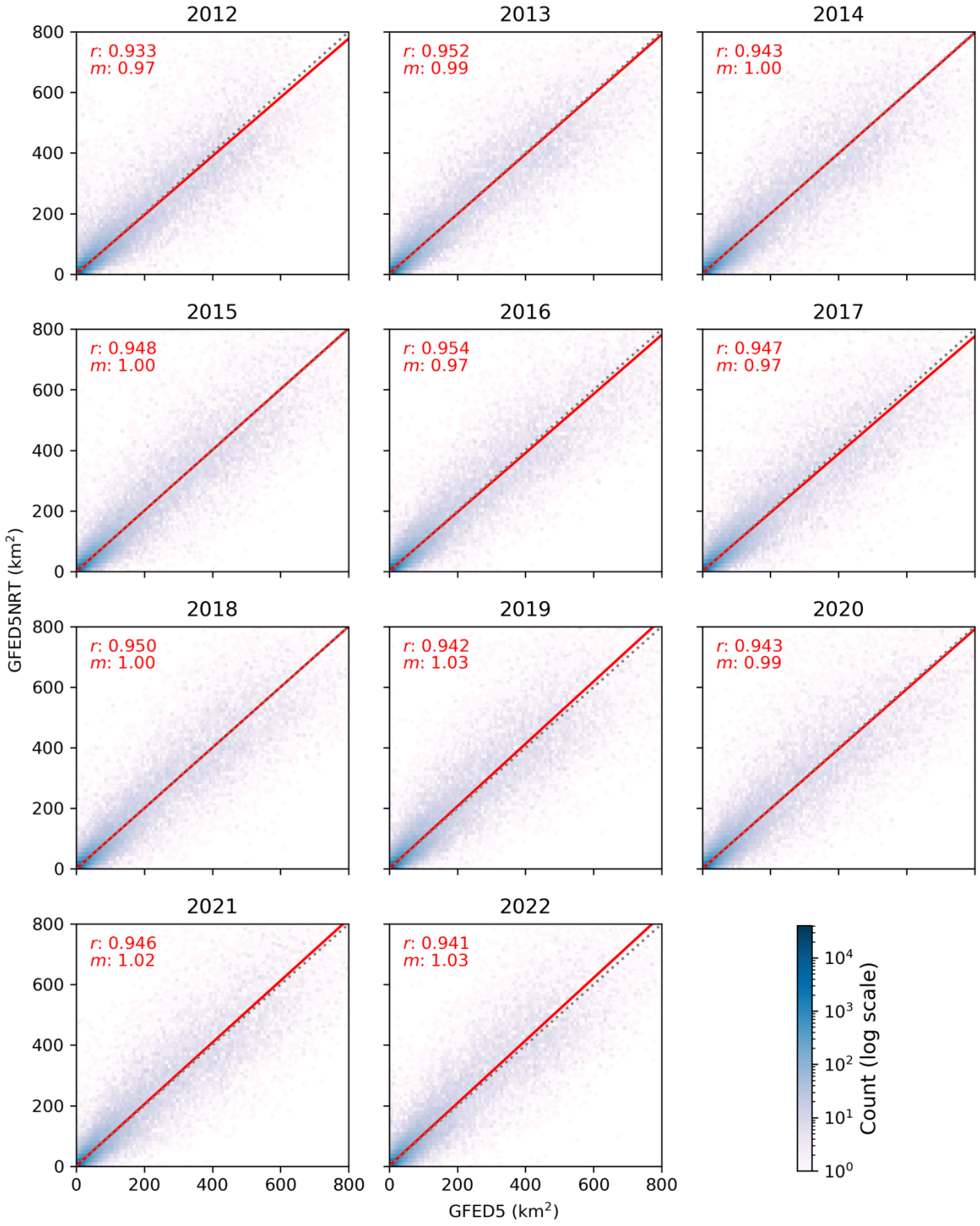

Figure S4. Global maps of total burned area in 2023 at 0.25° resolution from (a) GFED5NRT and (b) VIIRS SNPP.

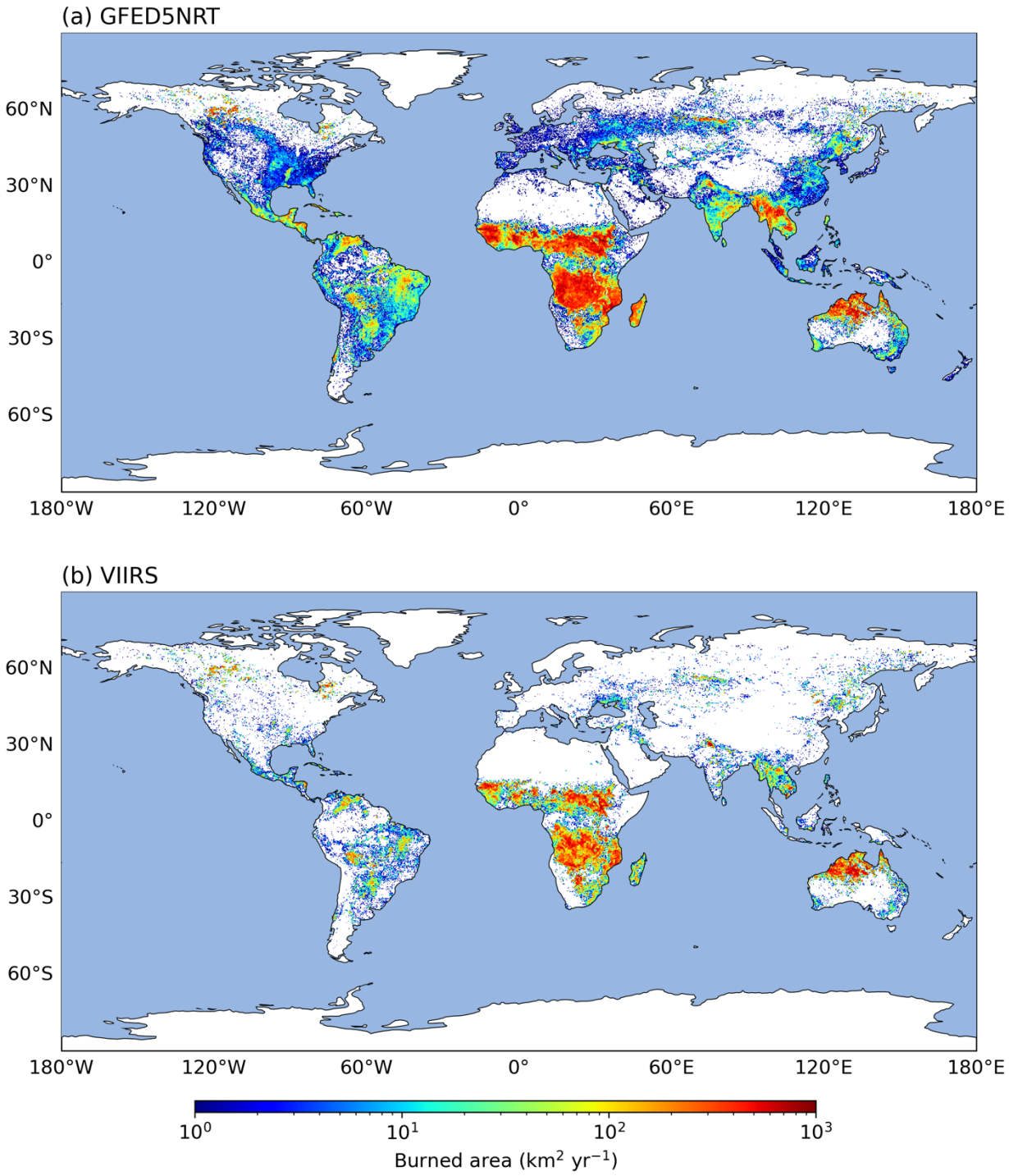

Figure S5. Comparison of annual burned area from GFED5 and GFED5NRT with independent regional datasets for 2002-2024 over (a) Canada and (b) Brazil. For GFED5NRT, the combined SNPP + NOAA-20 product is shown for 2023-2024, and the SNPP-only product for 2012-2022. Canadian comparisons include the Canadian National Fire Database (CNFDB; agency-reported fire perimeters) and the National Burned Area Composite (NBAC; Landsat-based burned area), as well as two independent 2023 estimates (NRCan_2023 and TIIC_2023). Brazilian comparisons include the INPE AQ1km product (MODIS-based burned area) and MapBiomas (Landsat-based). Crop-related burned area in GFED5 and GFED5NRT were excluded for Canada to ensure consistency with NBAC and CNFDB.

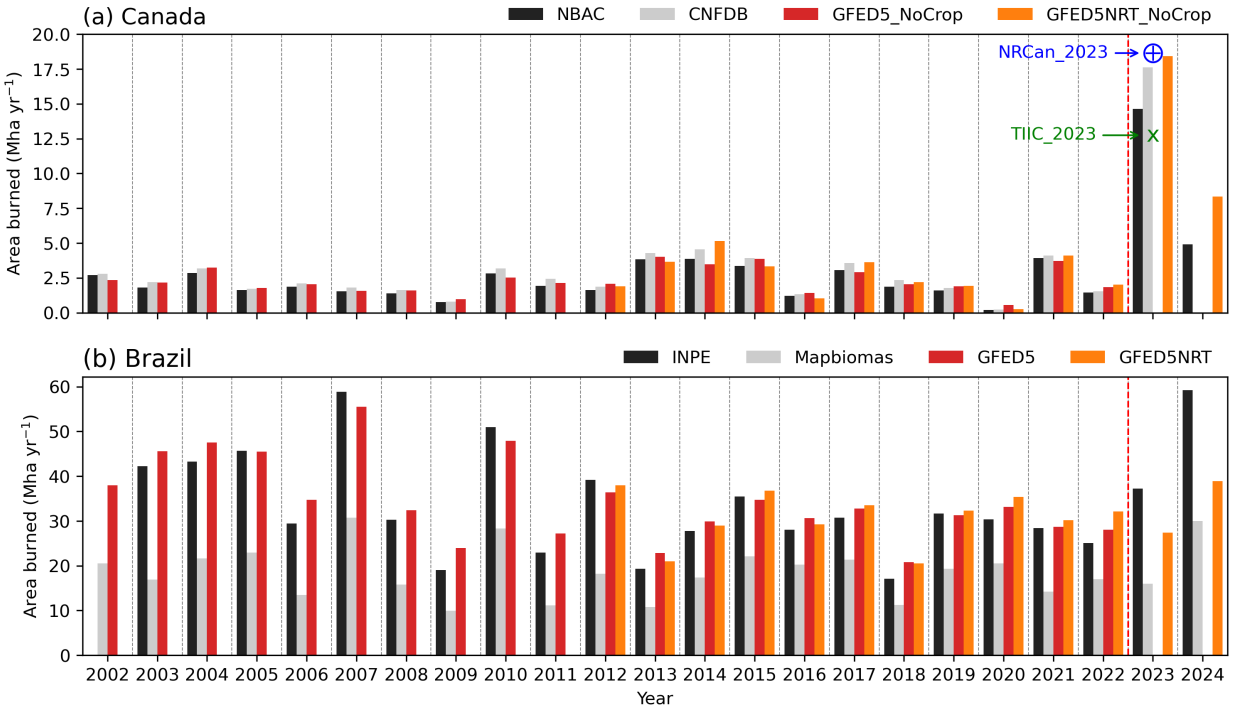

Figure S6. Monthly fire emissions averaged over 2023-2024 for 16 extreme-fire regions (see Figure 9 for the region boundaries), as estimated by GFED5NRT (red line). For reference, the climatologically mean (black line) and ±1 standard deviation range (gray shading) derived from GFED5 over 2002-2022 are also shown.

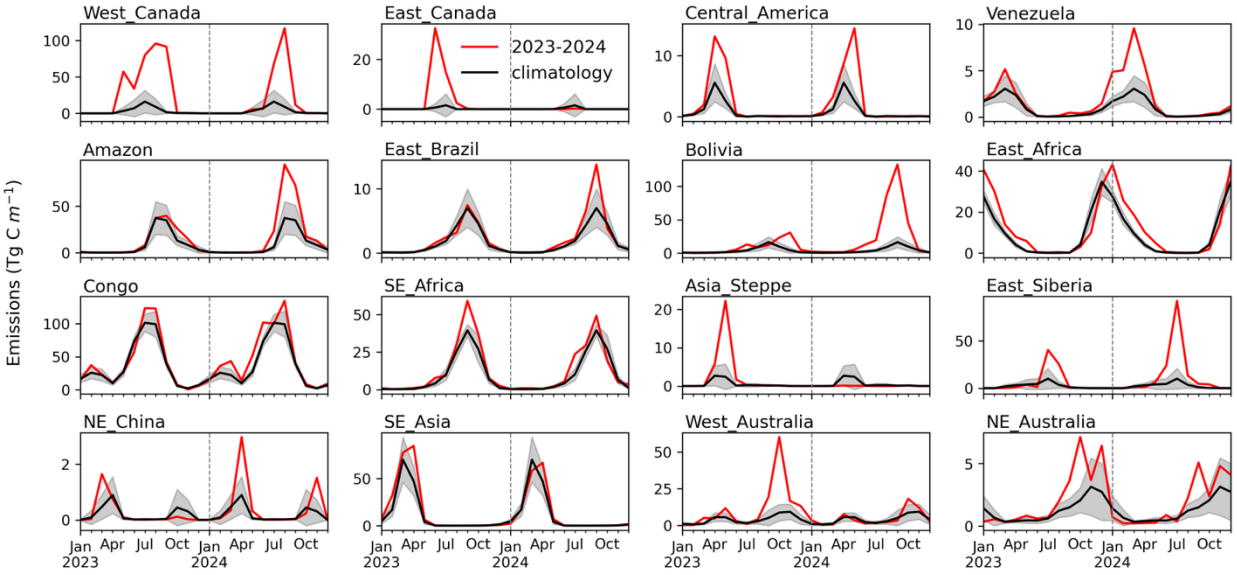

Figure S7. Extreme fire season in boreal North America during 2023 as depicted by GFED5NRT emission data. (a) Annual total emissions for 2023 and an example of regional daily emissions on September 23, 2023, at 0.25° resolution; (b) daily emission time series for 2023 compared with individual monthly time series and the mean for the historical (2002-2022) period; and (c) cumulative daily emissions for 2023 compared with the historical (2002-2022) range, defined by the maximum and minimum values.

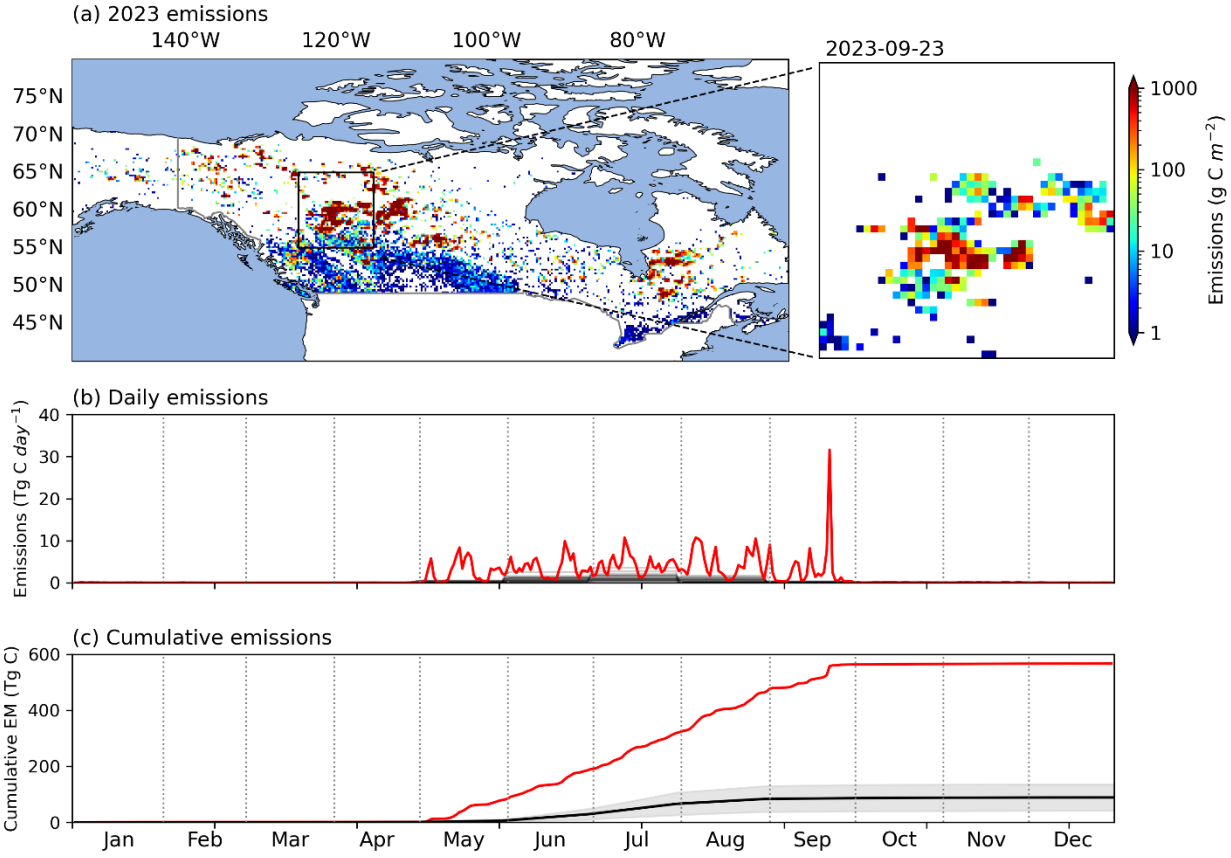

Figure S8. Extreme fire season in southern hemisphere South America during 2024 as depicted by GFED5NRT emission data. (a) Annual total emissions for 2024 and an example of regional daily emissions on September 7, 2024, at 0.25° resolution; (b) daily emission time series for 2024 compared with individual monthly time series and the mean for the historical (2002-2022) period; and (c) cumulative daily emissions for 2024 compared with the historical (2002-2022) range, defined by the maximum and minimum values.

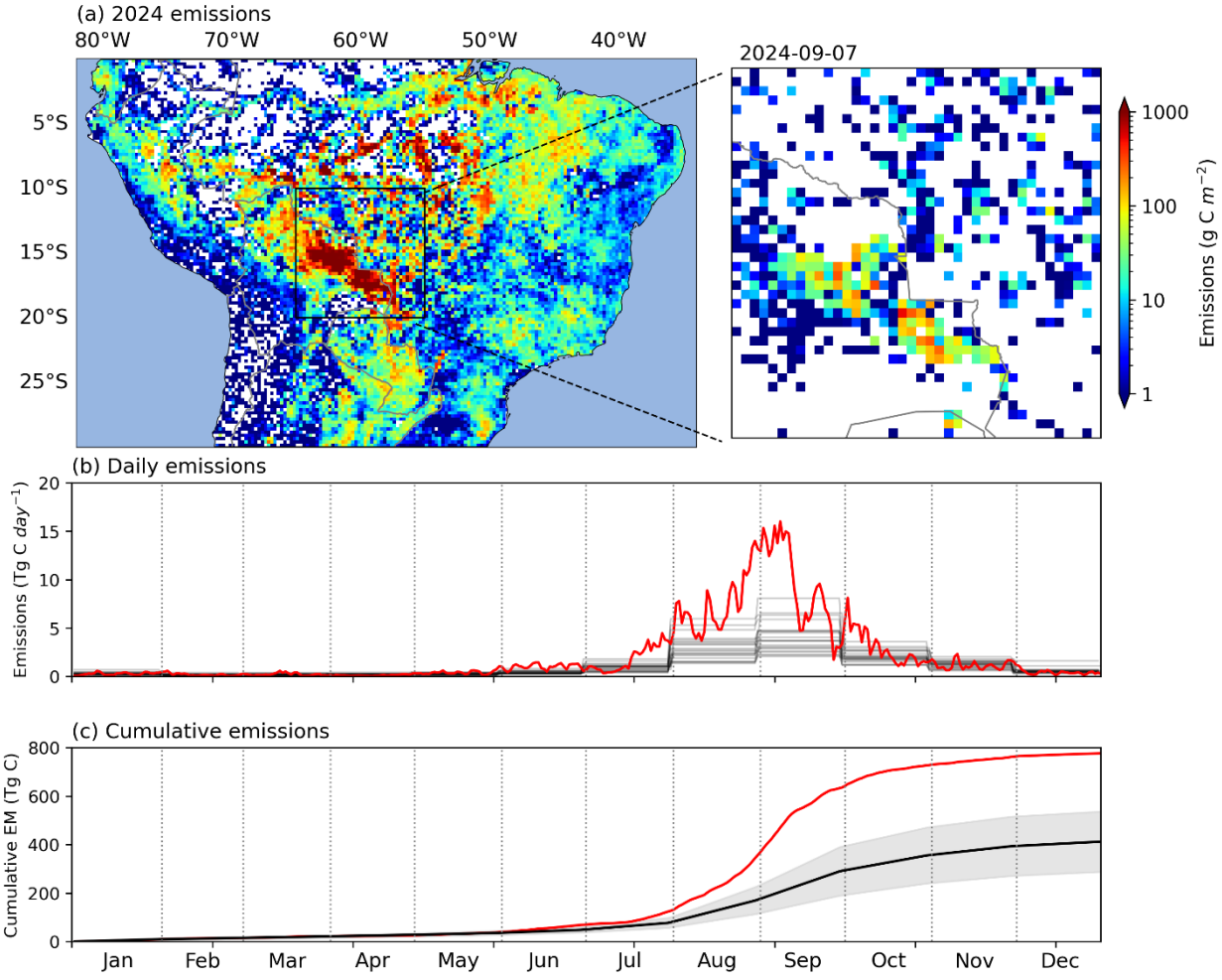

SI Text (S1-S4)

Text S1. Report-based static mask for identifying potential non-vegetation static hotspots

To help isolate biomass burning events, we integrated several global datasets to identify static thermal hotspots—persistent thermal anomalies unrelated to vegetation fires. These sources include active volcanism, gas flaring, landfills, industrial refineries, solar photovoltaic (PV) facilities, and power plants (geothermal and fossil fuel-based).

Any 0.01° grid cell containing one or more of these sources was classified as a "static cell" and masked from the VIIRS fire detection stream during the generation of the GFED5NRT product. The constituent datasets are summarized below:

- NOAA Global Gas Flaring **-** Flaring is commonly employed to dispose of excess natural gas at oil and gas production sites. The NOAA National Centers for Environmental Information (NCEI) and the Earth Observation Group (EOG) at the Colorado School of Mines developed the VIIRS Nightfire (VNF) product and a global gas flaring database (Elvidge et al., 2016; Zhizhin et al., 2021). This dataset includes flare locations and estimated emissions based on VIIRS thermal anomaly observations. The NOAA Global Gas Flaring data for (2012–2023) is available through the EOG website (https://eogdata.mines.edu/products/vnf/global_gas_flare.html).
- Volcanoes of the World (VOTW) -The Smithsonian Institution's Global Volcanism Program (GVP) maintains the Volcanoes of the World (VOTW) catalog (Global Volcanism Program et el., 2025), which documents Holocene volcanoes and their eruption histories. The current release, Version 5, is updated through 2023 and available from the GVP website (https://volcano.si.edu/gvp_votw.cfm).
- Global Power Plant Database - This comprehensive open-access Global Power Plant Database (Global Energy Observatory et al., 2021), maintained by the World Resources Institute (WRI), includes information on approximately 30,000 power plants across 164 countries. It spans a wide range of energy sources, including fossil fuels (coal, oil, gas), nuclear, biomass, geothermal, and renewables (solar, wind, hydro). The data are accessible through the WRI website (https://datasets.wri.org/datasets/global-power-plant-database).
- Global Inventory of Solar Energy Installations - The global inventory of solar photovoltaic generating units dataset (Kruitwagen et al., 2021) was developed by the University of Oxford, Descartes Labs, and the World Resources Institute (WRI). It is available for download through Zenodo (https://zenodo.org/records/5005868) and an online visualization tool is available at the Resource Watch data explorer (https://resourcewatch.org/data/explore/ene032-Solar-Plants_1).
- Oil and Gas Infrastructure Mapping (OGIM) Database - The OGIM database, developed by the Environmental Defense Fund (EDF) and MethaneSAT LLC, provides a harmonized global inventory of oil and gas infrastructure. It is constructed through the integration and QA/QC of publicly available geospatial datasets under a standardized schema and coordinate system. The methodology is detailed in (Omara et al., 2023), and the dataset is available via Zenodo (https://zenodo.org/records/13259749) and Google Earth Engine (https://developers.google.com/earth-engine/datasets/catalog/EDF_OGIM_current).

Text S2. Scaling weights to mitigate scan-angle bias

The VIIRS 375 m active fire product records individual thermal anomalies identified by sample and line numbers (Schroeder et al., 2014). The sample number (0–6399) corresponds to the sensor scan angle at the time of observation. However, fire detectability varies systematically across the VIIRS swath due to several factors:

- Geometric effects: Increases in pixel size and atmospheric path length at oblique angles.
- Environmental factors: Enhanced canopy obscuration at the swath edges.
- Algorithmic constraints: Scan-angle-dependent screening, such as sun-glint filtering.

These factors introduce a systematic bias in raw fire counts, which is particularly significant in daily analyses where scan-angle variations do not average out over time.

To normalize observed fire counts, we developed a sample-specific lookup table of weighting factors (*wgt*). These weights remove scan-angle dependence in detection frequency, ensuring that adjusted fire counts are statistically independent of the viewing geometry. Any residual variation is attributable to geometric effects related to pixel area and the VIIRS bowtie deletion scheme.

The weighting table was derived from a multi-year dataset of VIIRS detections (2019–2021). Detections were stratified by diurnal cycle (day/night), season (month), and dominant land cover within each 0.25° grid cell. For each stratum, the weight *wgt* for a given scan sample index *s* was calculated as:

$$wgt(s) = \beta / FireCount(s)$$

The normalization constant β was selected to conserve the total Fire Radiative Power (FRP; MW) within each stratum before and after adjustment. Since temporally integrated FRP is proportional to biomass-burning emissions (Freeborn et al., 2008; Wooster et al., 2013), this approach corrects detection biases while maintaining the integrity of emission estimates derived from the adjusted data.

Text S3. Data aggregation schemes for effective fire area and fuel consumption

We developed lookup tables for two scaling coefficients—effective fire area (EFA) and fuel consumption (FC)—using historical VIIRS active fire detections together with GFED5 burned area and fire emissions. To evaluate the sensitivity and robustness of these coefficients, we implemented a set of aggregation schemes (Table S2) that vary along three key dimensions: (1) spatial scale (0.25° grid cell, GFED region, or global), (2) temporal scale (monthly or annual means), and (3) treatment of fire type and biome (stratified by fire type or biome versus aggregated).

The resulting schemes span a continuum from highly generalized to highly stratified. At one extreme, the *Glb* scheme applies a single global scalar. At the other, more detailed configurations resolve variability by region, fire type, and time. The *Combine* scheme adopts a hybrid strategy to balances spatial detail and data availability: grid- and month-specific scalars (*Gridmo*) are where VIIRS detections are sufficient, while region- and type-specific monthly means (as in the *Regftpmo* scheme) are used in data-sparse areas.

Increasing stratification can improve representation of variability in fire behavior and emissions but also increases model complexity and the risk of overfitting. In regions with limited data, excessive stratification can amplify noise and reduce robustness, whereas simpler schemes are more stable but may overlook important spatial or temporal structure. An effective aggregation strategy therefore requires a balance between resolution and statistical support.

We evaluated all schemes by comparing burned area estimates scaled from VIIRS active fire counts (2012–2022) with GFED5. Performance metrics (Table S3), including normalized root mean square error (nRMSE), coefficient of determination (R^2), and bias, indicate that the *Regftp* scheme performs comparably to more complex alternatives while retaining a relatively low number of degrees of freedom. On this basis, *Regftp* was selected as the baseline scheme for GFED5NRT production.

Text S4. Identifying extreme fire events

We identified regional extreme fire events in 2023 and 2024 using gridded GFED5NRT fire emissions data. Annual fire emissions were aggregated for each year at 0.25° resolution, and a global map of mean annual emissions was constructed by averaging 2023 and 2024. Using the climatological mean and standard deviation of annual fire emissions from 2002–2022, we calculated grid cell level Z-scores (standardized anomalies) for 2023–2024.

Potential extreme fire regions were first identified as spatially contiguous clusters of grid cells exhibiting elevated Z-scores. These candidate regions were initially delineated based on visual inspection of the anomaly maps. For each candidate region, we refined its spatial extent by computing the concave hull enclosing all grid cells with Z-scores greater than 1 (i.e., exceeding one standard deviation above the climatological mean).

Finally, we calculated fire emission statistics within the refined boundaries of each extreme fire event region.

References

Chen, Y., Hall, J., van Wees, D., Andela, N., Hantson, S., Giglio, L., van der Werf, G. R., Morton, D. C., & Randerson, J. T. (2023). Multi-decadal trends and variability in burned area from the fifth version of the Global Fire Emissions Database (GFED5). *Earth System Science Data, 15*(11), 5227–5259. https://doi.org/10.5194/essd-15-5227-2023

Elvidge, C., Zhizhin, M., Baugh, K., Hsu, F.-C., & Ghosh, T. (2016). Methods for global survey of natural gas flaring from Visible Infrared Imaging Radiometer Suite data. *Energies*, *9*(1), 14. https://doi.org/10.3390/en9010014

Freeborn, P. H., Wooster, M. J., Hao, W. M., Ryan, C. A., Nordgren, B. L., Baker, S. P., & Ichoku, C. (2008). Relationships between energy release, fuel mass loss, and trace gas and aerosol emissions during laboratory biomass fires. *Journal of Geophysical Research: Atmospheres*, *113*(D1).

Giglio, L., van der Werf, G. R., Randerson, J. T., Collatz, G. J., & Kasibhatla, P. (2006). Global estimation of burned area using MODIS active fire observations. *Atmospheric Chemistry and Physics, 6*, 957–974. https://doi.org/10.5194/acp-6-957-2006

Giglio, L., Randerson, J. T., van der Werf, G. R., Kasibhatla, P. S., Collatz, G. J., Morton, D. C., & DeFries, R. S. (2010). Assessing variability and long-term trends in burned area by merging multiple satellite fire products. *Biogeosciences*, *7*(3), 1171–1186.

Global Energy Observatory, Google, KTH Royal Institute of Technology in Stockholm, Enipedia, & World Resources Institute. (2021). *Global Power Plant Database* (Version 1.3.0) [Data set]. World Resources Institute. https://datasets.wri.org/datasets/global-power-plant-database

Global Volcanism Program. (2025). *Volcanoes of the World* (E. Venzke, Comp.; Version 5.3.4) [Data set]. Smithsonian Institution. https://doi.org/10.5479/si.GVP.VOTW5-2025.5.3

Kruitwagen, L., Story, K. T., Friedrich, J., Byers, L., Skillman, S., & Hepburn, C. (2021). A global inventory of photovoltaic solar energy generating units. *Nature*, *598*(7882), 604–610. https://doi.org/10.1038/s41586-021-03957-7

Omara, M., Gautam, R., O'Brien, M. A., Himmelberger, A., Franco, A., Meisenhelder, K., Hauser, G., Lyon, D. R., Chulakadabba, A., Miller, C. C., Franklin, J., Wofsy, S. C., & Hamburg, S. P. (2023). Developing a spatially explicit global oil and gas infrastructure database for characterizing methane emission sources at high resolution. *Earth System Science Data*, *15*(8), 3761–3790. https://doi.org/10.5194/essd-15-3761-2023

Schroeder, W., Oliva, P., Giglio, L., & Csiszar, I. A. (2014). The New VIIRS 375m active fire detection data product: Algorithm description and initial assessment. *Remote Sensing of Environment*, *143*, 85–96. https://doi.org/10.1016/j.rse.2013.12.008

van der Werf, G. R., Randerson, J. T., Giglio, L., Collatz, G. J., Kasibhatla, P. S., & Arellano, A. F. (2006). Interannual variability in global biomass burning emissions from 1997 to 2004. *Atmospheric Chemistry and Physics, 6*(11), 3423–3441. https://doi.org/10.5194/acp-6-3423-2006

van der Werf, G. R., Randerson, J. T., Giglio, L., Collatz, G. J., Mu, M., Kasibhatla, P. S., Morton, D. C., DeFries, R. S., Jin, Y., & van Leeuwen, T. T. (2010). Global fire emissions and the contribution of deforestation, savanna, forest, agricultural, and peat fires (1997–2009). *Atmospheric Chemistry and Physics, 10*(23), 11707–11735. https://doi.org/10.5194/acp-10-11707-2010

van der Werf, G. R., Randerson, J. T., Giglio, L., van Leeuwen, T. T., Chen, Y., Rogers, B. M., Mu, M., van Marle, M. J. E., Morton, D. C., Collatz, G. J., Yokelson, R. J., & Kasibhatla, P. S. (2017). Global fire emissions estimates during 1997–2016. *Earth System Science Data, 9*(2), 697–720. https://doi.org/10.5194/essd-9-697-2017

van der Werf, G. R., Randerson, J. T., van Wees, D., Chen, Y., Giglio, L., Hall, J., Roland, V., Mu, M., Binte Shahid, S., Barsanti, K. C., Yokelson, R., & Morton, D. C. (2025). Landscape fire emissions from the 5th version of the Global Fire Emissions Database (GFED5). *Scientific Data*, *12*(1), 1870. https://doi.org/10.1038/s41597-025-06127-w

Wooster, M. J., Roberts, G., Smith, A. M., Johnston, J., Freeborn, P., Amici, S., & Hudak, A. T. (2013). Thermal remote sensing of active vegetation fires and biomass burning events. In *Thermal Infrared Remote Sensing* (pp. 347–390). Springer.

Zhizhin, M., Matveev, A., Ghosh, T., Hsu, F.-C., Howells, M., & Elvidge, C. (2021). Measuring gas flaring in Russia with multispectral VIIRS Nightfire. *Remote Sensing*, *13*(16), 3078. https://doi.org/10.3390/rs13163078